

1                    **Moulin density controls the timing of peak**  
2                    **pressurization within the Greenland Ice Sheet’s**  
3                    **subglacial drainage system**

4                    **J. Z. Mejia<sup>1</sup>, J. D. Gulley<sup>2</sup>, C. Trunz<sup>3</sup>, M. D. Covington<sup>4</sup>, T. C.**  
5                    **Bartholomaus<sup>5</sup>, C. Breithaupt<sup>6</sup>, S. Xie<sup>7</sup>, T. H. Dixon<sup>2</sup>**

6                    <sup>1</sup>Department of Geology, University at Buffalo, Buffalo, NY 14260

7                    <sup>2</sup>Department of Geosciences, University of South Florida, Tampa, FL 33620.

8                    <sup>3</sup>Department of Applied Geomatics, Université de Sherbrooke, Sherbrooke, QC J1K 2R1

9                    <sup>4</sup>Department of Geosciences, University of Arkansas, Fayetteville, AR 72701

10                    <sup>5</sup>Department of Earth and Spatial Sciences, University of Idaho, Moscow, ID 83844

11                    <sup>6</sup>Exxonmobil Upstream Research Company, Spring, TX 77389

12                    <sup>7</sup>Department of Civil and Environmental Engineering, University of Houston, Houston, TX 77204

13                    **Key Points:**

- 14                    • Larger catchments within the Greenland Ice Sheet’s ablation area impart signif-  
15                    icant delays on the timing of meltwater delivery to moulins  
16                    • Peak moulin head occurred 1–3.25 hours later at higher elevations  
17                    • Peak moulin head and sliding speeds are not coincident where moulin density is  
18                    low

---

Corresponding author: Jessica Mejía, [jzmejia@buffalo.edu](mailto:jzmejia@buffalo.edu)

**Abstract**

Links between hydrology and sliding of the Greenland Ice Sheet (GrIS) are poorly understood. Here, we monitored meltwater’s propagation through the entire glacial hydrologic system for catchments at different elevations by quantifying the lag cascade as daily meltwater pulses traveled through the supraglacial, englacial, and subglacial drainage systems. We found that meltwater’s residence time within supraglacial catchments—depending upon area, snow cover, and degree of channelization—controls the timing of peak moulin head, resulting in the two hour later peak observed at higher-elevations. Unlike at lower elevations where peak moulin head and sliding coincided, at higher elevations peak sliding lagged moulin head by  $\sim 2.8$  hours. This delay was likely caused by the area’s lower moulin density, which required diurnal pressure oscillations to migrate further away from subglacial conduits to elicit the observed velocity response. These observations highlight the supraglacial drainage system’s control on coupling GrIS hydrology and sliding.

**Plain Language Summary**

Each summer, melting snow and ice collects within stream and rivers on the Greenland Ice Sheet’s surface until reaching crevasses or moulins—near-vertical conduits that penetrate the entire ice thickness—where this meltwater can lubricate the bed, causing the overlying ice to slide more rapidly. Despite the important role of meltwater in modulating sliding speeds, little is known about how relationships between melting and sliding vary spatially or through time. Here, we take the novel approach of monitoring meltwater’s propagation through the entire glacial hydraulic system at two elevations. We find that longer delays in the timing of meltwater delivery to moulins draining larger, higher-elevation catchments, caused peak moulin water level (i.e., peak pressurization) to occur two hours later in the day than at smaller, lower-elevation catchments. Unlike at lower elevations where peak moulin water level and sliding coincided, at higher elevations sliding lagged peak moulin water level by 2.8 hours. This delay was likely caused by the fewer number of moulins which require a single moulin to pressurize a larger proportion area. This work reveals the importance of the supraglacial drainage system in imparting controlling the timing of meltwater reaching the bed and its relationship with sliding.

**1 Introduction**

Accurate predictions of the Greenland Ice Sheet’s (GrIS) future contributions to sea level rise require a good understanding of the dynamic links between melting, subglacial water pressures, and ice motion. Meltwater produced on the ice sheet’s surface flows through complex networks of supraglacial streams and rivers that ultimately empty into crevasses or moulins (Rennermalm et al., 2013; Smith et al., 2015; Yang & Smith, 2016). Moulins are vertical conduits that penetrate the entire ice thickness and connect to the most efficient parts of the dynamic subglacial drainage system (Gulley et al., 2012). Meltwater inputs to moulins modulate subglacial water pressures and basal traction, which controls sliding (Andrews et al., 2014; Bartholomaus et al., 2007). Accordingly, the supraglacial, englacial, and subglacial drainage systems are inherently linked, meaning that changes in any of these components can impact ice motion. Despite the hydraulic system’s interconnections, most studies of glacial hydrological systems have focused on one component at a time, resulting in critical gaps in our understanding of links between changes in hydrology and ice motion.

Large scale ice sheet models exclude key components of the glacial hydrologic system when investigating the ice-dynamic response to melting (Goelzer et al., 2020). Frequently, the supraglacial drainage system is overlooked under the assumption that meltwater delivery to the subglacial drainage system is coincident with peak melting across the ablation area. Such simplifications contrast with observations that reveal significant heterogeneity in the timing of meltwater delivery to moulins (King, 2018; Yang & Smith,

2016; Yang et al., 2018), which can lag peak melting by up to 16 hours for the largest catchments (Smith et al., 2017). Observations show temporal lags between peak melting and peak sliding speeds increase with elevation and distance from the ice sheet’s margin (Hoffman et al., 2011), suggesting there should be spatiotemporal differences in the hydro-dynamic coupling throughout the GrIS ablation area. These lags are likely caused by longer delays in the timing of meltwater delivery to moulins with larger catchment areas, which similarly increase with elevation as moulin density decreases (Clason et al., 2015; Yang et al., 2018). Even though the importance of meltwater inputs on sliding is well documented, how differences in the timing of meltwater delivery to moulins and their spatial distribution impact sliding has not been fully investigated.

Here we take a novel and holistic approach to understanding relationships between melting and sliding on the GrIS by quantifying lags in meltwater propagation through each component of the glacial hydraulic system. We established two field camps at different elevations—a lower elevation field camp, Low Camp, and a higher-elevation camp, High Camp—where we measured the timing of daily peaks in melting, meltwater delivery to moulins, moulin hydraulic head (the water level within the moulin with respect to sea level), and surface ice velocity. We use these observations to investigate how differences in the physical characteristics of supraglacial drainage basins control lags between peak meltwater production and delivery to moulins and how these differences impact sliding.

## 2 Data and Methods

### 2.1 Field Sites

In July 2017, we established two camps within the ablation area of Sermeq Avannarleq in west Greenland: a lower elevation site *Low Camp* and a higher-elevation site *High Camp* at elevations of 779 and 947 m.a.s.l., respectively (Figure 1; Table S2; Ice thicknesses of 503 and 790 m (Morlighem et al., 2017)). We monitored meltwater propagation within an internally drained catchment at each elevation, the moulins of which we refer to as JEME (at Low Camp), and RAD1 (at High Camp) (Figure 1b–c). To constrain the timing and magnitude of daily melting we installed an automatic weather station at each camp (Text S4), supplementing our observations with data from the nearby GCNET station JAR1 (Figure 1; Steffen et al., 1996). We monitored the timing of meltwater delivery to each catchment’s terminal moulin using ultrasonic water level sensors positioned approximately 30 m upstream of each moulin (Figures S1–S4). We measured moulin water level by directly instrumenting moulins with pressure transducers, allowing us to monitor pressure fluctuations within the most hydraulically connected parts of the subglacial drainage system. On 21 July we instrumented Low Camp’s JEME moulin (69.474°N, -49.825°E) which drained  $\sim 0.2$  km<sup>2</sup> (Figure 1; Table S1). On 29 July we instrumented High Camp’s Radical moulin (RAD1; 69.543°N, -49.693°E) which drained  $\sim 16.7$  km<sup>2</sup> (Figure 1; Tables S1 and S3). Finally, we monitored ice motion by installing several global navigation satellite system (GNSS) stations at both camps (Text S6).

In 2018 we returned to the field to expand our observations. Before the onset of melting, we installed a seismic station to measure glaciohydraulic tremor amplitude, a proxy for the discharge and pressure gradient within subglacial conduits (Text S7; Bartholomaeus et al., 2015; Gimbert et al., 2016), within Low Camp’s main catchment JEME. On 10 July, we instrumented the newly formed PIRA moulin which drained the same catchment as JEME moulin the previous year (catchment area  $\sim 0.2$  km<sup>2</sup>; Figure S3). PIRA moulin formed in approximately the same location as JEME moulin was before it had advected  $\sim 90$  m downglacier over the winter. To further constrain catchment area induced delays in meltwater delivery to moulins, we instrumented two auxiliary catchments with supraglacial stream gauges: JNIH catchment at Low Camp (July 2017; area  $\sim 1.1$  km<sup>2</sup>), and SBPI catchment at High Camp (August 2018;  $\sim 2.4$  km<sup>2</sup>; Figure 1).

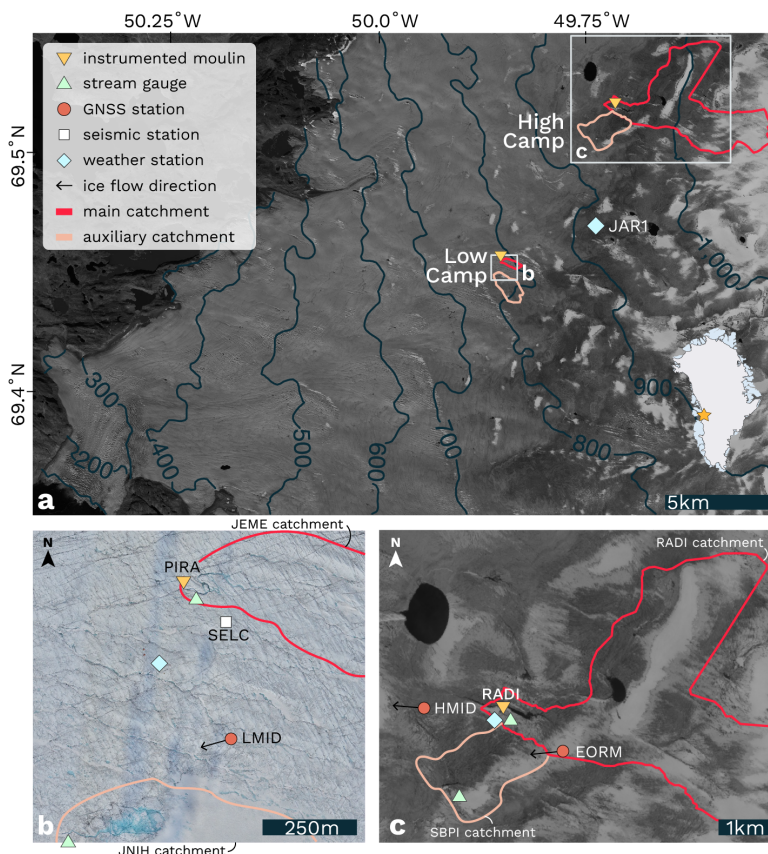


**Figure 1. Sermeq Avannarleq field sites.** (a) Sentinel-2 imagery from 10 Aug 2018 showing the full extent of the catchments studied at Low Camp and High Camp. (b) July 2018 drone orthophoto showing Low Camp, our main catchment JEME is outlined in red. PIRA (yellow triangle) and JEME moulins draining this catchment were located in the same position in 2017 and 2018 (Figures S1, S3–S4). (c) High Camp zoom in showing instrumented moulin RADI (yellow) with outlined catchment (Figures S2 and S5).

### 3 Results

The instruments deployed during the 2017 and 2018 melt seasons allowed us to monitor and constrain the timing of meltwater propagation through the glacial hydraulic system for catchments at Low Camp and High Camp. We deployed the first instruments in July 2017 after the melt season had already begun and the snowline had retreated past both our lower and higher-elevation sites.

#### 3.1 Meltwater production

We used recorded meteorological measurements and the enhanced temperature-index model by Pellicciotti et al. (2005) to calculate melt rates to constrain the timing of peak meltwater production (Text S3; Figures 3a, S9a–S11a). Melting peaked simultaneously across our study area (Figure 2), occurring around  $13:30 \pm 1.4$  hours local time (henceforth all times are reported in local time (UTC-02:00)). The timing and magnitude of peak melting was most strongly correlated with incoming solar radiation (Text S3). A comparison between calculated melt rate and ice surface ablation recorded at Low Camp (Text S3; 13 July–19 August 2017) shows good agreement with peak ablation occurring  $13:30 \pm$

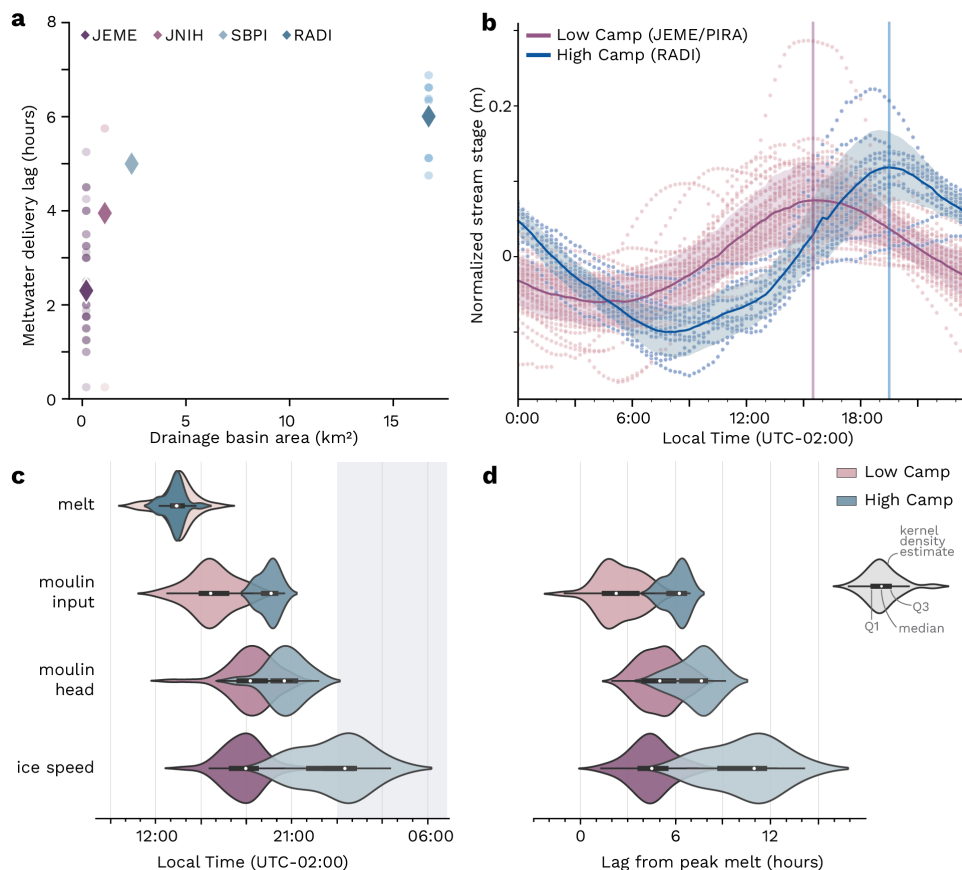


**Figure 2.** (a) Peak melting to meltwater delivery lag with respect to catchment area. Diamonds mark mean values with dots representing individual observations. (b) Normalized daily supraglacial stream stage for our catchments at Low Camp (purple) and High Camp (blue) primary catchments. The mean timing of diurnal peaks are marked with vertical lines. (c) Box plots overlaid by height-normalized kernel density estimates showing the timing of peak melting, meltwater delivery to moulins, moulin head, and ice speed for Low Camp (purple) and High Camp (Blue) during the 2017 melt season. (d) same as in c but shown as lag from peak melting.

135 3.5 hours (Figures S7–S8). Over the same time period air temperature peaked two hours  
 136 later, around  $15:30 \pm 3.3$  hours (Figure S7). Moreover, peak melting occurred consistently  
 137 around 13:30 at both Low Camp and High Camp over the 2017 and 2018 melt seasons.  
 138 Due to the similarity in observations between weather stations, we use a single timeseries  
 139 of peak melting to quantify lags across all variables.

### 140 3.2 Meltwater delivery to moulins

141 Of the physical characteristics considered, catchment area exerted the strongest control  
 142 on the timing of peak meltwater delivery to moulins. At Low Camp’s main catchment  
 143 JEME ( $0.2 \text{ km}^2$ ), meltwater delivery peaked around 15:30 (Figure 2b–c), lagging  
 144 peak melt by  $2.4 \pm 1.6$  hours over the period of 2 July–9 August 2017 (Figure 2d; Table  
 145 S3). At High Camp’s much larger RAD catchment ( $16.8 \text{ km}^2$ ), meltwater delivery  
 146 peaked around 19:45, lagging peak melt by  $6.5 \pm 1.8$  hours (Figure 2 and S11) over the  
 147 period of 5–16 August 2017. The longer residence time of meltwater within the supra-  
 148 glacial drainage system at the larger, higher-elevation RAD catchment ultimately caused

149 moulin input to peak four hours later in the day at RADI when compared to the smaller  
 150 and lower-elevation JEME catchment (Figure 2b–c). Importantly, all of the underlying  
 151 data used to generate the aforementioned timing of peak meltwater delivery for JEME  
 152 and RADI catchments were collected during bare-ice conditions (see Figures S1 and S2  
 153 for photos of surface conditions). Bare-ice conditions therefore eliminate the influence  
 154 of the seasonal snowpack on the timing of peak meltwater to moulins reported here.

155 Observations from our two auxiliary catchments confirm the pattern of longer lags  
 156 between peak melting and peak meltwater delivery to moulins with increased catchment  
 157 area (Figure 2a; Table S1). At Low Camp’s JNIIH (1.1 km<sup>2</sup>; 13–20 July 2017) peak melt-  
 158 water delivery lagged peak melting by  $4.2 \pm 1.8$  hours, and by  $5.0 \pm 1.3$  hours at High  
 159 Camp’s SBPI (2.4 km<sup>2</sup>; August 2018). Altogether, observations from four catchments  
 160 indicate there are increasing delays in the timing of meltwater delivery to larger, higher-  
 161 elevation catchments (Figure 2a) within this sector of the western GrIS.

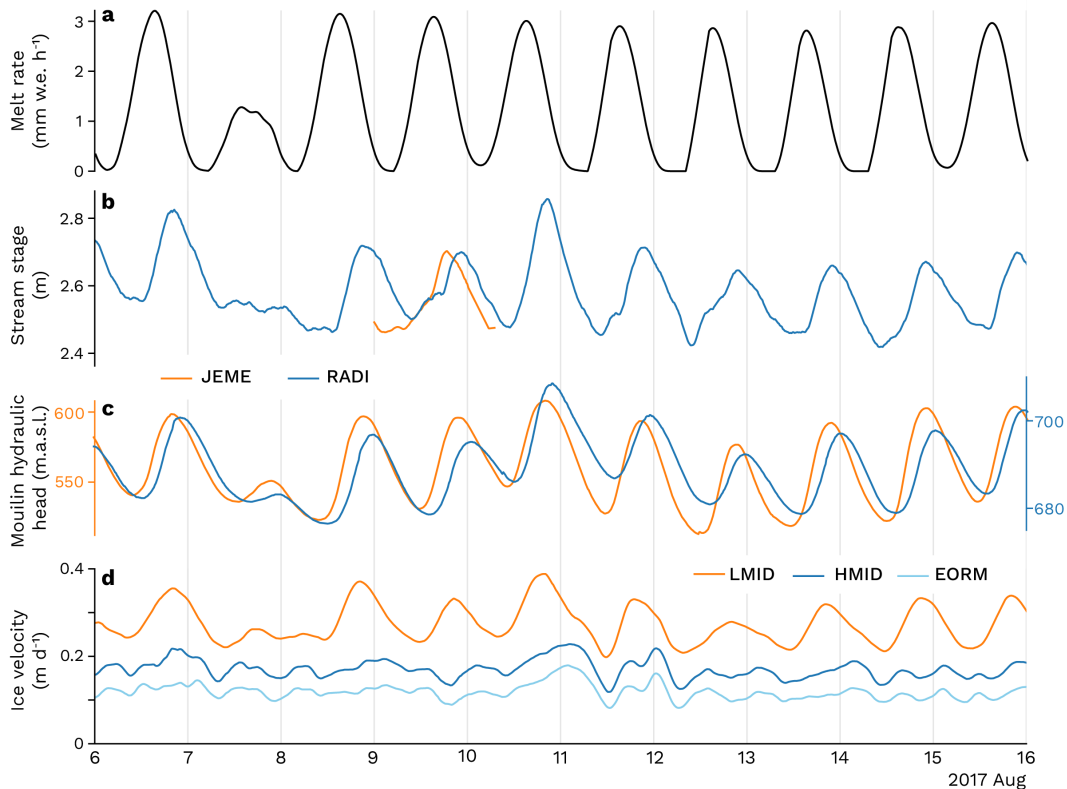


**Figure 3.** Comparison between Low Camp measurements (orange) and High Camp measurements (blue). (a) Meltwater production (b) supraglacial stream stage about an arbitrary datum. (c) Moulin hydraulic head from JEME moulin (left axis, orange) and RADI moulin (right axis, blue). The two axes are shown to highlight the phase-shift between the two timeseries (see Figure S12 for a single axes). (d) Along-flow ice velocity. Extended timeseries are shown in Figures S9 and S11.

### 162 3.3 Moulin hydraulic head and sliding

163 Coincident timeseries of moulin head from August 2017 (Figures 3, S9c–S11c) con-  
 164 strain the timing of peak pressures within the subglacial drainage system for Low Camp  
 165 and High Camp moulins. The lag between peak meltwater delivery to moulins and peak

166 moulin head was similar, approximately two hours, at both sites (Figures 2c–d and S15).  
 167 However, the longer delay in meltwater delivery caused High Camp’s RADI moulin’s water  
 168 level to peak 1–3.25 hours later in the day than at the lower-elevation JEME moulin  
 169 (Figure S15). This delay resulted in a clear phase shift between the moulin head time-  
 170 series from JEME and RADI moulins (Figure 3c).

171 We find a strong agreement between the timing of peak moulin head and peak slid-  
 172 ing speed at Low Camp that is not observed at High Camp. For example, peak sliding  
 173 speed at Low Camp coincided with peak moulin head but lagged peak melting by  $4.6 \pm$   
 174  $1.7$  hours (Figure 2d). This pattern was observed during 2017 and 2018 with peak slid-  
 175 ing lagging peak moulin head by  $-0.4 \pm 1.5$  hours ( $n = 21$ ) for JEME and  $-0.3 \pm$   
 176  $2.3$  hours ( $n = 28$ ) for PIRA (i.e., sliding precedes head). In contrast, at High Camp  
 177 peak sliding lagged (i.e. followed) peak moulin head by  $2.8 \pm 2.0$  and  $3.0 \pm 1.2$  hours for  
 178 GNSS stations EORM and HMID respectively. Ultimately sliding peaked 2.2–7.6 hours  
 179 later at High Camp than at Low Camp throughout the 2017 melt season (Figure 3d).

### 180 3.4 Glacio-hydraulic tremor amplitude

181 To investigate how transient surface conditions (i.e., seasonal snowpack removal and  
 182 supraglacial drainage network evolution) within Low Camp’s JEME catchment influence  
 183 the timing of meltwater delivery to moulins, we utilize observations of glacio-hydraulic  
 184 tremor amplitude to supplement stream stage observations which only cover 11 July and  
 185 20 August 2018 during bare-ice conditions (Figure 4 and S10). Our tremor amplitude  
 186 timeseries spanned the entire duration of the melt season, from 5 June through the end  
 187 of August 2018 ( $n = 62$  for diurnal extrema picks). Peak meltwater delivery to PIRA  
 188 moulin coincided with peak tremor amplitude (Figure S13; Text S4 and S7), which oc-  
 189 curs when subglacial pressure gradients within moulin-connected subglacial channels are  
 190 increasing most rapidly (Gimbert et al., 2016). From the monthly breakdown of diurnal  
 191 extrema peaks shown in Figure 4, tremor amplitude peaked earlier in the day as the melt  
 192 season progressed, lagging peak melting by  $6.1 \pm 2.2$ ,  $3.5 \pm 2.5$ , and  $1.4 \pm 2.5$  hours in  
 193 June, July, and August respectively. Stream stage observations agree, with the lag be-  
 194 tween peak melting and peak meltwater delivery decreasing by 54 minutes between July  
 195 and August 2018.

## 196 4 Discussion

### 197 4.1 Controls on the timing of peak moulin head

198 By constraining the timing of peak meltwater delivery to moulins within five GrIS  
 199 catchments, we show that differences in the physical characteristics of catchments—area,  
 200 snowpack extent, and supraglacial drainage efficiency—induce non-trivial heterogeneity  
 201 in the timing of meltwater delivery to moulins. Lags between peak melting and peak melt-  
 202 water delivery to moulins increased with catchment area (Figure 2a), resulting in longer  
 203 delays in the timing of meltwater delivery to larger, higher-elevation catchments. This  
 204 is expected because meltwater must be transported greater distances over the ice sur-  
 205 face before reaching the catchment’s terminal moulin (Sherman, 1932). Previous works  
 206 have shown a positive relationship between catchment area and delays in meltwater de-  
 207 livery through applying traditional hydrological theory to supraglacial catchment through-  
 208 out the GrIS ablation area (King, 2018; Smith et al., 2017; Yang & Smith, 2016; Yang  
 209 et al., 2018). In considering 799 catchments in SW Greenland, Smith et al. (2017) showed  
 210 that catchments with areas 0.4–244.9 km<sup>2</sup> could produce lags between peak melting and  
 211 meltwater delivery to moulins of 0.4–9.5 hours. Our observations show that even a more  
 212 limited range of catchment sizes (0.2–16.8 km<sup>2</sup>) can induce differences of over four hours  
 213 in the timing of meltwater delivery to moulins, thereby inducing a similar offset in tim-  
 214 ing of peak moulin head across the ablation area.

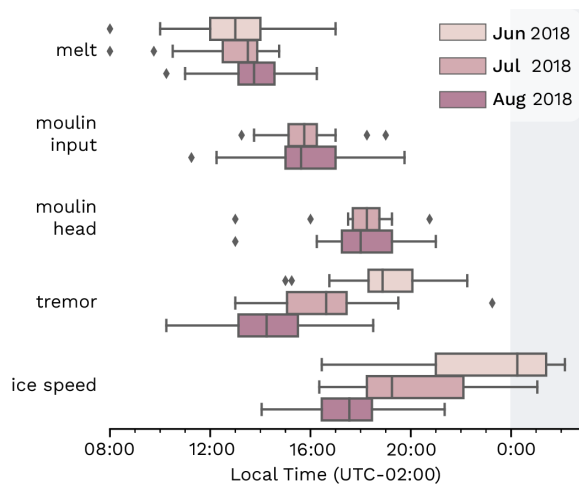


**Figure 4.** Seasonal shifts in meltwater propagation timing. Box and whisker plots show the monthly distribution of daily peaks in melting, meltwater input to PIRA moulin (stream stage), PIRA moulin head, tremor amplitude, and ice speed of Low Camp’s JEME catchment during the 2018 melt season. Shading corresponding to the month of the underlying data for June (lightest), July (mid-tone), and August (darkest). Gray diamonds mark outliers, and the center line corresponds to median values. Shading as in Figure 2.

215 The timing of meltwater delivery to moulins within individual catchments evolves  
 216 over the course of the melt season as the seasonal snowpack melts and then as efficient  
 217 supraglacial stream networks form (Lampkin & Vanderberg, 2014; Willis et al., 2002; Yang  
 218 et al., 2018). Early in the 2018 melt season (i.e., the first few weeks following the melt  
 219 season’s initiation on 6 June), snow cover was likely responsible for the increase in melt-  
 220 water’s residence time within the supraglacial drainage system as indicated by the differ-  
 221 ence in peak tremor amplitude and sliding velocity between June and July (Figure  
 222 4). This increased residence time would have delayed meltwater delivery to the Low Camp  
 223 moulin PIRA during the first few weeks of the 2018 melt season as the snowline quickly  
 224 retreated upglacier (Text S9). This approximately three hour increase is similar to pre-  
 225 vious work on Haut Glacier d’Arolla’s La Vierge catchment (0.11 km<sup>2</sup>) where Willis et  
 226 al. (2002) showed the seasonal snowpack could increase the lag between peak melting  
 227 and peak meltwater delivery by more than two hours. Despite being snow-free by July  
 228 2018, peak meltwater delivery to PIRA moulin decreased by 1–1.75 hours between July  
 229 and August. This shorter residence time of meltwater within the supraglacial drainage  
 230 system is likely attributed to increased supraglacial drainage density where small trib-  
 231 utaries drain into well-developed streams and rivers which quickly transport meltwater  
 232 to the catchment’s terminal moulin (e.g., Yang & Smith, 2016).

233 By including direct measurements of moulin head within the primary catchments  
 234 considered in this study, we identified a two hour lag between peak meltwater delivery  
 235 and moulin head. The lag between peak meltwater delivery and moulin head was con-  
 236 sistent throughout the melt season and between sites despite significant differences in  
 237 the magnitude and timing of peak meltwater delivery to the moulins themselves (Fig-  
 238 ure 2c–d). This contrasts previous assumptions that peak meltwater delivery and moulin  
 239 head would occur simultaneously (e.g., McGrath et al., 2011). While our observations  
 240 cannot be extrapolated to every moulin on the GrIS, they do demonstrate that there is  
 241 a delay inherent to the coupled englacial-subglacial drainage system that controls the  
 242 absolute timing of peak moulin head and therefore the timing of peak pressurization within  
 243 moulin-connected parts of the subglacial drainage system.

244

## 4.2 Local relationships between effective pressure and ice motion

245

246

247

248

249

250

251

252

253

254

255

256

Lags between peak melting and peak sliding speed increased with distance from the ice sheet margin, echoing the pattern established by Hoffman et al. (2011). At Low Camp, peak moulin head and peak sliding speed were nearly coincident, indicating daily peaks in moulin head control the timing of peak subglacial water pressure and sliding. At High Camp, longer delays in meltwater delivery caused moulin head to peak 1–3.25 hours later than at Low Camp (Figure 3). However, this delay does not entirely account for the later timing of peak sliding, which lagged peak moulin head by up to 3.5 hours. Accordingly, the timing of peak moulin head was only partially responsible for the later timing of peak sliding. Instead the timing offset between peak pressure within the moulin-connected drainage system and peak sliding speed indicates there is a difference in the relationship between effective pressure (ice overburden pressure minus subglacial water pressure) and sliding at higher elevations that was not observed lower on the ice sheet.

257

258

259

260

261

262

263

264

265

266

267

268

269

270

271

272

273

274

275

276

277

278

279

The spatial distribution and density of moulins control the development of the subglacial drainage system by determining where meltwater is delivered to the bed and thus where subglacial conduits form (Banwell et al., 2016; Gulley et al., 2012). When moulin head is high, subglacial conduits become pressurized relative to the surrounding distributed drainage system, driving water out laterally away from the conduits and into neighboring linked-cavities (Bartholomaus et al., 2007; Hubbard et al., 1995; Rada & Schoof, 2018; Werder et al., 2013). As higher pressures migrate out into the distributed system, basal traction is reduced over a larger area of the bed, thereby promoting sliding. Because sliding is controlled by the areally integrated basal traction over three to eight ice thicknesses (Gudmundsson, 2003), peak sliding should occur when high pressures cover the largest area of the bed. At lower elevations on the ice sheet where moulin density is high (e.g., Low Camp’s primary catchment with more than 10 moulins per km<sup>2</sup>; Figure S4), closely spaced subglacial conduits work in tandem to quickly pressurize a large area of the bed. However, at higher elevations where moulin density is much lower (e.g., High Camp with 1–3 moulins per km<sup>2</sup>; Figure S5), sliding will be more coupled to the pressure change emanating from an individual conduit as it migrates into the distributed system. Modeling work by Werder et al. (2013) showed that the diurnal pressurization of a single conduit can extend up to two kilometers into the distributed system, with the water pressure perturbation amplitude decreasing with distance away from the conduit, while also incurring a progressive phase lag of up to six hours. In this paradigm, the finite diffusion speed of the pressure change within the conduit at the base of RADI moulin could produce the two hour lag between peak moulin head and peak sliding observed at our higher-elevation site.

280

## 4.3 Implications

281

282

283

284

285

286

287

288

289

290

291

292

293

294

Our results reinforce previous observations of spatially inhomogeneous patterns of GrIS ice motion driven by areas with direct hydraulic connections to the bed, while highlighting the added complexity induced by the differences in timing of peak moulin head throughout the ablation area. Longitudinal flow coupling acts over a range of length-scales, explaining acceleration in areas of the GrIS without direct hydraulic connections to the bed (Price et al., 2008; Ryser et al., 2014). Areas without direct hydraulic connections (i.e., without moulins), respond passively to ice motion induced by pressure fluctuations within moulin-connected parts of the subglacial drainage system (Ryser et al., 2014). At our lower elevation site, moulin head and sliding speeds peaked consistently earlier than at higher elevations. Accordingly, when peak pressurization (or “slipperiness”) was reached at lower elevations, upglacier areas were still resisting flow, and vice versa. This observed offset in the timing of peak pressurization may then produce different patterns of ice deformation, stress transfer, and basal motion, than would be expected if all areas with moulins experienced peak pressurization coincidentally.

295 Alpine glaciers have been frequently used as analogues to the GrIS, yet their use-  
296 fulness remains a point of debate. Fundamental relationships between hydrology and ice  
297 motion identified within alpine environments diverge with distance inland as the ice thick-  
298 ens, surface slopes flatten, and moulin density decreases. Our results demonstrate the  
299 correlation between moulin head and peak sliding initially identified on alpine glaciers  
300 (Iken, 1972) seems to hold in areas with high moulin density (e.g., Low Camp). This re-  
301 lationship likely remains intact in this area because closely-spaced moulins are able to  
302 feed water simultaneously to the entirety of the ice sheet bed (Andrews et al., 2014). How-  
303 ever, at higher elevations where moulin density is low (e.g., High Camp), the same cor-  
304 relation between moulin head and peak sliding is not observed. Accordingly, the straight-  
305 forward coupling between effective pressure and ice motion derived from studies on alpine  
306 glaciers breaks down for inland reaches of the GrIS ablation area. Resolving the distinct  
307 processes governing hydrodynamic coupling within these areas will be more important  
308 as the GrIS ablation area continues to expand further inland as the climate warms (Noël  
309 et al., 2019).

## 310 5 Conclusions

311 Our observations suggest the supraglacial drainage system controls hydrodynamic  
312 coupling by two mechanisms: by creating delays in meltwater routing that propagate through  
313 the englacial and subglacial drainage systems and by controlling the spatial distribution  
314 of moulins which affects relationships between effective pressure and sliding. Because moulin  
315 density and catchment area are inherently linked, these processes work together to pro-  
316 duce the progressively later timing daily peak sliding speeds with increasing distance from  
317 the ice sheet’s margin. Given the role of the supraglacial drainage system in controlling  
318 the timing of peak subglacial pressurization, we would expect the well-documented het-  
319 erogeneity of supraglacial catchments (King, 2018; Smith et al., 2017; Yang & Smith, 2016)  
320 to produce widespread variability in the timing of peak pressurization experienced within  
321 different regions of the subglacial drainage system. How these complex patterns of sub-  
322 glacial pressurization influence ice flow need to be considered in order to determine how  
323 the GrIS will respond to increased melting under future climatic warming.

## 324 Acknowledgments

325 This work was supported by the United States National Science Foundation grant num-  
326 ber 1604022. GNSS station support was provided by UNAVCO in collaboration with the  
327 National Science Foundation. Thank you to Victoria Siegel and Ronald Knoll for assis-  
328 tance in the field. Polar Field Services, Inc. provided logistical support, and special thanks  
329 to Kathy Young for her work supporting field campaigns. ArcticDEM provided by the  
330 Polar Geospatial Center under NSF-OPP awards 1043681, 1559691, and 1542736. DEM(s)  
331 were created from DigitalGlobe, Inc., imagery and funded under National Science Foun-  
332 dation awards 1043681, 1559691, and 1542736.

## 333 Data Availability Statement

334 The data sets and code used in this study are openly available. Meteorological and hy-  
335 drological data sets are archived with the National Science Foundation’s Arctic Data Cen-  
336 ter through the MoVE project’s portal: <http://arcticdata.io/catalog/portals/moulin>  
337 (Mejia, Trunz, Covington, & Gulley, 2020; Mejia, Trunz, Covington, Gulley, & Breithaupt,  
338 2020; Mejia et al., 2021). GC-Net weather station data from JAR1 is available from (Steffen  
339 et al., 1996) and is also archived with (Mejia et al., 2021) for convenience. Data from  
340 our on-ice GNSS stations and the base stations used during processing are archived through  
341 UNAVCO’s GAGE Facility (Fahnestock et al., 2006; Mejia, Gulley, & Dixon, 2020). The  
342 Python module created to pick diurnal extrema is archived with Zenodo (see Mejia, 2022).

## References

- 343  
344 Andrews, L. C., Catania, G. A., Hoffman, M. J., Gulley, J. D., Lüthi, M. P., Ryser,  
345 C., . . . Neumann, T. A. (2014). Direct observations of evolving subglacial  
346 drainage beneath the Greenland Ice Sheet. *Nature*, *514*(7520), 80–83. doi:  
347 10.1038/nature13796
- 348 Banwell, A. F., Hewitt, I. J., Willis, I. C., & Arnold, N. S. (2016). Moulin  
349 density controls drainage development beneath the Greenland ice sheet.  
350 *Journal of Geophysical Research: Earth Surface*, *121*(12), 2248–2269. doi:  
351 10.1002/2015JF003801
- 352 Bartholomäus, T. C., Anderson, R. S., & Anderson, S. P. (2007). Response of glacier  
353 basal motion to transient water storage. *Nature Geoscience*, *1*, 33–37. doi: 10  
354 .1038/ngeo.2007.52
- 355 Bartholomäus, T. C., Larsen, C. F., Amundson, J. M., O’Neel, S., Walter, J. I.,  
356 & West, M. E. (2015). Subglacial discharge at tidewater glaciers revealed  
357 by seismic tremor. *Geophysical Research Letters*, *42*, 6391–6398. doi:  
358 10.1002/2015GL064590
- 359 Clason, C. C., Mair, D. W., Nienow, P. W., Bartholomew, I., Sole, A. J., Palmer, S.,  
360 & Schwanghart, W. (2015). Modelling the transfer of supraglacial meltwater to  
361 the bed of Leverett Glacier, Southwest Greenland. *Cryosphere*, *9*(1), 123–138.  
362 doi: 10.5194/tc-9-123-2015
- 363 Fahnestock, M. A., Truffer, M., SDFE, T. D. A., & Community, U. (2006). *Greenland*  
364 *GNSS Network - KAGA-Kangia North P.S.*. UNAVCO. doi: 10.7283/FQGY  
365 -4535
- 366 Gimbert, F., Tsai, V. C., Bartholomäus, T. C., Amundson, J. M., & Walter, J. I.  
367 (2016). Subseasonal changes observed in subglacial channel pressure, size, and  
368 sediment transport. *Geophysical Research Letters*, *43*(September), 3786–3794.  
369 doi: 10.1002/2016GL068337
- 370 Goelzer, H., Nowicki, S., Payne, A., Larour, E., Seroussi, H., Lipscomb, W. H., . . .  
371 Van Den Broeke, M. (2020). The future sea-level contribution of the Greenland  
372 ice sheet: A multi-model ensemble study of ISMIP6. *Cryosphere*, *14*, 3071–3096.  
373 doi: 10.5194/tc-14-3071-2020
- 374 Gudmundsson, G. H. (2003). Transmission of basal variability to a glacier surface.  
375 *Journal of Geophysical Research: Solid Earth*, *108*(B5), 1–19. doi: 10.1029/  
376 2002jb002107
- 377 Gulley, J. D., Grabiec, M., Martin, J. B., Jania, J., Catania, G. A., & Glowacki,  
378 P. S. (2012). The effect of discrete recharge by moulins and heterogeneity  
379 in flow-path efficiency at glacier beds on subglacial hydrology. *Journal of*  
380 *Glaciology*, *58*(211), 926–940. doi: 10.3189/2012JoG11J189
- 381 Hoffman, M. J., Catania, G. A., Neumann, T. A., Andrews, L. C., & Rumrill, J. A.  
382 (2011). Links between acceleration, melting, and supraglacial lake drainage  
383 of the western Greenland Ice Sheet. *Journal of Geophysical Research: Earth*  
384 *Surface*, *116*(4), 1–16. doi:10.1029/2010JF001934
- 385 Hubbard, B., Sharp, M. J., Willis, I. C., Nielsen, M. K., & Smart, C. (1995). Borehole  
386 water-level variation and the structure of the subglacial hydrological system  
387 of Haut Glacier d’Arolla, Valais, Switzerland. *Journal of Glaciology*, *41*(139),  
388 572–583.
- 389 Iken, A. (1972). Measurements of Water Pressure In Moulins as Part of A Move-  
390 ment Study of the White Glacier, Axel Heiberg Island, Northwest Territories,  
391 Canada. *Journal of Glaciology*, *11*(61), 53–58.
- 392 King, L. A. (2018). *Identifying and characterizing the spatial variability of supraglacial*  
393 *hydrological features on the western Greenland Ice Sheet* (Doctoral dissertation,  
394 University of British Columbia). doi: 10.14288/1.0372827
- 395 Lampkin, D. J., & Vanderberg, J. (2014). Supraglacial melt channel networks in the  
396 Jakobshavn Isbræ region during the 2007 melt season. *Hydrological Processes*,  
397 *28*(25), 6038–6053. doi: 10.1002/hyp.10085

- 398 McGrath, D., Colgan, W. T., Steffen, C., Lauffenburger, P., & Balog, J. (2011). As-  
 399 sessing the summer water budget of a moulin basin in the sermeq avannarleq  
 400 ablation region, Greenland ice sheet. *Journal of Glaciology*, *57*(205), 954–964.  
 401 doi: 10.3189/002214311798043735
- 402 Mejia, J. Z. (2022, July). *jzmeja/diurnalextrama: v1.0.0*. Zenodo. Retrieved from  
 403 <https://doi.org/10.5281/zenodo.6812156> doi: 10.5281/zenodo.6812156
- 404 Mejia, J. Z., Gulley, J. D., & Dixon, T. H. (2020). *West Greenland Moulines 2017-*  
 405 *2019 Sermeq Avannarleq - GPS/GNSS Observations Dataset*. The GAGE Fa-  
 406 cility operated by UNAVCO, Inc. doi: 10.7283/VT31-EK40
- 407 Mejia, J. Z., Gulley, J. D., Trunz, C., Covington, M. D., Bartholomaeus, T. C., Xie,  
 408 S., & Dixon, T. (2021). Isolated cavities dominate Greenland Ice Sheet dy-  
 409 namic response to lake drainage. *Geophysical Research Letters*, 1–11. doi:  
 410 10.1029/2021gl094762
- 411 Mejia, J. Z., Trunz, C., Covington, M. D., & Gulley, J. D. (2020). *Meteorological*  
 412 *data from two on-ice weather stations at 780 and 950 m asl elevations in the*  
 413 *ablation area of Sermeq Avannarleq, West Greenland from 2017-2018*. Arctic  
 414 Data Center. doi: 10.18739/A2CF9J745
- 415 Mejia, J. Z., Trunz, C., Covington, M. D., Gulley, J. D., & Breithaupt, C. (2020).  
 416 *Moulin hydrological measurements from Sermeq Avannarleq, West Greenland*  
 417 *Ice Sheet from 2017-2018*. Arctic Data Center. doi: 10.18739/A2M03XZ13
- 418 Morlighem, M., Williams, C. N., Rignot, E., An, L., Arndt, J. E., Bamber, J. L., ...  
 419 Zinglensen, K. B. (2017). BedMachine v3: Complete Bed Topography and  
 420 Ocean Bathymetry Mapping of Greenland From Multibeam Echo Sounding  
 421 Combined With Mass Conservation. *Geophysical Research Letters*, *44*(21),  
 422 11,051–11,061. doi: 10.1002/2017GL074954
- 423 Noël, B., van de Berg, W. J., Lhermitte, S., & van den Broeke, M. R. (2019). Rapid  
 424 ablation zone expansion amplifies north Greenland mass loss. *Science Advances*,  
 425 *5*(9), 2–11. doi: 10.1126/sciadv.aaw0123
- 426 Pellicciotti, F., Brock, B., Strasser, U., Burlando, P., Funk, M., & Corripio, J.  
 427 (2005). An enhanced temperature - index glacier melt model including the  
 428 shortwave radiation balance : development and testing for Haut Glacier  
 429 d ' Arolla , Switzerland. *Journal of Glaciology*, *51*(175), 573 – 587. doi:  
 430 10.3189/172756505781829124
- 431 Price, S. F., Payne, A. J., Catania, G. A., & Neumann, T. A. (2008). Seasonal acceler-  
 432 ation of inland ice via longitudinal coupling to marginal ice. *Journal of Glaciol-*  
 433 *ogy*, *54*(185), 213–219. doi: 10.3189/002214308784886117
- 434 Rada, C., & Schoof, C. (2018). Channelized, distributed, and disconnected: subglacial  
 435 drainage under a valley glacier in the Yukon. *The Cryosphere*, *12*(8), 2609–2636.  
 436 Retrieved from <https://doi.org/10.5194/tc-12-2609-2018> doi: 10.5194/tc-  
 437 12-2609-2018
- 438 Rennermalm, Å. K., Moustafa, S. E., Mioduszewski, J., Chu, V. W., Forster, R. R.,  
 439 Hagedorn, B., ... Tedesco, M. (2013). Understanding Greenland ice sheet  
 440 hydrology using an integrated multi-scale approach. *Environmental Research*  
 441 *Letters*, *8*(1). doi: 10.1088/1748-9326/8/1/015017
- 442 Ryser, C., Lüthi, M. P., Andrews, L. C., Catania, G. A., Funk, M., & Hawley, R. L.  
 443 (2014). Caterpillar-like ice motion in the ablation zone of the Greenland ice  
 444 sheet. *Journal of Geophysical Research : Earth Surface*, *119*, 2258–2271. doi:  
 445 10.1002/2013JF003067.Received
- 446 Sherman, L. K. (1932). The Relation of Hydrographs of Runoff to Size and Character  
 447 of Drainage-Basins. *Eos, Transactions American Geophysical Union*, *13*(1), 332–  
 448 229.
- 449 Smith, L. C., Chu, V. W., Yang, K., Gleason, C. J., Pitcher, L. H., Rennermalm,  
 450 Å. K., ... England, J. H. (2015). Efficient meltwater drainage through  
 451 supraglacial streams and rivers on the southwest Greenland ice sheet. *Pro-*  
 452 *ceedings of the National Academy of Sciences*, *112*(4), 1001–1006. doi:

- 453 10.1073/pnas.1413024112  
454 Smith, L. C., Yang, K., Pitcher, L. H., Overstreet, B. T., Chu, V. W., & Renner-  
455 malm, Å. K. (2017). Direct measurements of meltwater runoff on the Greenland  
456 ice sheet surface. *Proceedings of the National Academy of Sciences*, *114*(50),  
457 1–10. doi: 10.1073/pnas.1707743114
- 458 Steffen, C., Box, J. E., & Abdalati, W. (1996). Greenland Climate Network: GC-Net.  
459 *Cold Regions Research and Engineering Laboratory, CRREL Spec*, 98–103.
- 460 Werder, M. A., Hewitt, I. J., Schoof, C., & Flowers, G. E. (2013). Modeling channel-  
461 ized and distributed subglacial drainage in two dimensions. *Journal of Geophys-  
462 ical Research: Earth Surface*, *118*(4), 2140–2158. doi: 10.1002/jgrf.20146
- 463 Willis, I. C., Arnold, N. S., & Brock, B. W. (2002). Effect of snowpack removal on  
464 energy balance, melt and runoff in a small supraglacial catchment. *Hydrological  
465 Processes*, *16*(14), 2721–2749. doi: 10.1002/hyp.1067
- 466 Yang, K., & Smith, L. C. (2016). Internally drained catchments dominate supraglacial  
467 hydrology of the southwest Greenland Ice Sheet. *Journal of Geophysical Re-  
468 search : Earth Surface*, *121*, 1891–1910. doi: 10.1002/2016JF003927
- 469 Yang, K., Smith, L. C., Karlstrom, L., Cooper, M. G., Tedesco, M., & van As, D.  
470 (2018). A new surface meltwater routing model for use on the Greenland Ice  
471 Sheet surface. *The Cryosphere*, *12*, 3791–3811. doi: 10.5194/tc-12-3791-2018